Journal of Sound and Vibration (2000) **237**(4), 617–640
doi:10.1006/jsvi.2000.3071, available online at http://www.idealibrary.com on IDEAL®

NON-LINEAR DYNAMICS AND STABILITY OF CIRCULAR CYLINDRICAL SHELLS CONTAINING FLOWING FLUID. PART III: TRUNCATION EFFECT WITHOUT FLOW AND EXPERIMENTS

M. Amabili

Dipartimento di Ingegneria Industriale, Università di Parma, Parco Area delle Scienze 181/*A*, *Parma, I* - 43100 *Italy. E-mail: marco@me.unipr.it*

F. Pellicano

Dipartimento di Scienze dell'Ingegneria, Università di Modena e Reggio Emilia, Via Campi 213/*B*, *Modena I* - 41100, *Italy*

AND

M. P. Païdoussis

Department of Mechanical Engineering, McGill University, 817 *Sherbrooke Street W., Montreal, Québec, Canada H3A* 2*K*6

(*Received* 13 *September* 1999, *and in final form* 20 *March* 2000)

The response of simply supported circular cylindrical shells to harmonic excitation in the spectral neighbourhood of one of the lowest natural frequencies is investigated by using improved mode expansions with respect to those assumed in Parts I and II of the present study. Two cases are studied: (1) shells *in vacuo*; and (2) shells filled with stagnant water. The improved expansions allow checking the accuracy of the solutions previously obtained and giving definitive results within the limits of Donnell's non-linear shallow-shell theory. The improved mode expansions include: (1) harmonics of the circumferential mode number n under consideration, and (2) only the principal n, but with harmonics of the longitudinal mode included. The effect of additional longitudinal modes is absolutely insignificant in both the driven and companion mode responses. The effect of modes with $2n$ circumferential waves is very limited on the trend of non-linearity, but is significant in the response with companion mode participation in the case of lightly damped shells (empty shells). In particular, the travelling wave response appears for much lower vibration amplitudes and presents a frequency range without stable responses, corresponding to a beating phenomenon. A liquid (water) contained in the shell generates a much stronger softening behaviour of the system. Experiments with a water-filled circular cylindrical shell made of steel are in very good agreement with the present theory.

1. INTRODUCTION

The response of simply supported circular cylindrical shells to a harmonic excitation in the spectral neighbourhood of one of the lowest natural frequencies is investigated by using improved mode expansions with respect to those assumed in Parts I and II [1, 2] of the present study. Two cases are studied: (1) shells *in vacuo*; (2) shells filled with stagnant water. The improved expansions allow checking the accuracy of the solutions previously obtained

0022-460X/00/440617 + 24 $35.00/0

and giving definitive results within the limits of Donnell's non-linear shallow-shell theory [3].

The harmonic excitation is assumed to be in the neighbourhood of the mode (n, m) of the shell having prevalent radial displacement, where n is the number of circumferential waves and m is the number of axial half-waves. In particular, the case $m = 1$, $n > 0$ (asymmetric mode) without fluid flow is considered in this paper. The improved mode expansions include either: (1) harmonics of the circumferential mode number n under consideration, or (2) only the principal n, but with harmonics of the longitudinal mode included.

Results confirm the supposition made in Part II of the present study [2], i.e., that additional terms in the mode expansion do not have the same fundamental effect on the trend of non-linearity as the first and third axisymmetric modes. The effect of additional longitudinal modes is absolutely insignificant in both the driven and companion mode responses. The effect of modes with harmonics of the circumferential mode number n under consideration is limited on the trend of non-linearity but is significant in the response with companion mode participation for lightly damped shells (empty shells). In particular, the travelling wave response appears for much lower vibration amplitudes and presents a frequency range without stable responses, corresponding to a beating phenomenon.

A complete review of studies on large-amplitude vibrations of circular cylindrical shells is given by Amabili *et al.* [4, 5]. In particular, two of these previous studies used modal expansions of radial displacement including modes with $2n$ circumferential waves to study the non-linear shell response: Ginsberg [6] and Chen and Babcock [7]. However, they condensed the model to a two degree-of-freedom (d.o.f.) one by using a perturbation approach with some kind of truncation error. No studies showing the effect of truncation of mode expansion in the non-linear shell response are available.

Experiments with a water-filled circular cylindrical shell made of steel have given results in very good agreement with the present theory. Experimental data for shell response larger than the shell thickness are rare in literature.

2. ADDITIONAL TERMS IN THE MODE EXPANSION

Similar to Parts I and II [1, 2] of the present study, attention is focused on both a finite, simply supported, closed circular cylindrical shell of length L, and an infinitely long shell, periodically supported. A cylindrical co-ordinate system (O; x, r, θ) is chosen, with the origin O placed at the centre of one end of the shell. The displacements of points in the middle surface of the shell are denoted by u, v and w, in the axial, circumferential and radial directions respectively. Using Donnell's non-linear shallow-shell theory, the equation of motion for large-amplitude transverse vibrations of a very thin, circular cylindrical shell is given by [1, 3]

$$D\nabla^4 w + ch\dot{w} + \rho h\ddot{w} = f - p + \frac{1}{R}\frac{\partial^2 F}{\partial x^2} + \left(\frac{\partial^2 F}{R^2\partial\theta^2}\frac{\partial^2 w}{\partial x^2} - 2\frac{\partial^2 F}{R\,\partial x\,\partial\theta}\frac{\partial^2 w}{R\,\partial x\,\partial\theta} + \frac{\partial^2 F}{\partial x^2}\frac{\partial^2 w}{R^2\,\partial\theta^2}\right), \tag{1}$$

where $D = Eh^3/[12(1-\nu^2)]$ is the flexural rigidity, E is Young's modulus, ν the Poisson ratio, h the shell thickness, R the mean shell radius, ρ the mass density of the shell, c (kg/m^3/s) the damping coefficient, and f and p are the radial pressures applied to the surface of the shell as a consequence of external forces and the contained flowing fluid

respectively. The radial deflection w is positive inward, $\dot{w} = (\partial w/\partial t)$, $\ddot{w} = (\partial^2 w/\partial t^2)$; F is the in-plane stress function, given by [1, 3]

$$\frac{1}{Eh}\nabla^4 F = -\frac{1}{R}\frac{\partial^2 w}{\partial x^2} + \left[\left(\frac{\partial^2 w}{R\,\partial x\,\partial\theta}\right)^2 - \frac{\partial^2 w}{\partial x^2}\frac{\partial^2 w}{R^2\,\partial\theta^2}\right]. \tag{2}$$

In equations (1) and (2) the biharmonic operator is defined as $\nabla^4 = [\partial^2/\partial x^2 + \partial^2/(R^2\partial\theta^2)]^2$. In Parts I and II of the present study [1, 2] the following mode expansion of the flexural deformation w has been used:

$$w(x, \theta, t) = \sum_{m=1}^{2} [A_{m,n}(t)\cos(n\theta) + B_{m,n}(t)\sin(n\theta)]\sin(\lambda_m x) + \sum_{m=1}^{3} A_{(2m-1),0}(t)\sin(\lambda_{(2m-1)}x), \tag{3}$$

where $\lambda_m = m\pi/L$, $A_{m,n}(t)$, $B_{m,n}(t)$ and $A_{m,0}(t)$ are unknown functions of time t. Equation (3) was obtained by neglecting the interaction between the asymmetric mode considered and other asymmetric modes of different n. Moreover, the interaction among asymmetric modes with different numbers of longitudinal half-waves is stopped at $m = 2$; in particular, it was observed [2] that without fluid flow there is no interaction between modes $(n, 1)$ and $(n, 2)$. The role of axisymmetric modes in non-linear vibrations of the shell was deeply studied in Part II of the present study [2]; axisymmetric modes with m even can be eliminated in the expansion, because they do not contribute to shell contraction. It was shown [2], however, that it is necessary to retain the first and third axisymmetric modes, i.e. (0, 1) and (0, 3), and that it is possible to neglect other axisymmetric modes in the study of the harmonic response of mode $(n, 1)$ of a shell without flow. In order to have more complete results on the accuracy of the mode expansion used in the present study, it was considered useful to investigate (1) the interaction among asymmetric modes with different n and (2) the interaction among asymmetric modes of the same n but different m.

The harmonic response without flow is considered here; the driven (directly excited) mode considered has one longitudinal half-wave: $m = 1$, for any n. From the structure of the equations, where quadratic and cubic non-linearities appear, and for symmetry reasons (rotating the system by $2\pi/n$ is expected to give the same system configuration) the interaction among asymmetric modes of different n will be possible only with modes having kn circumferential waves, where k is an integer. Here $k = 1, 2$ is considered to evaluate the truncation effect in the series expansion. Analogously, for symmetry reasons, the interaction among asymmetric modes with different numbers of longitudinal half-waves involves only odd values of m [2]; in particular, $m = 1, 3$ is considered.

The effect on the dynamics of modes with $2n$ circumferential waves is investigated by using the following mode expansion:

$$w(x, \theta, t) = \sum_{k=1}^{2} [A_{m,kn}(t)\cos(kn\theta) + B_{m,kn}(t)\sin(kn\theta)]\sin(m\pi x/L) + \sum_{m=1}^{2} A_{(2m-1),0}(t)\sin(\lambda_{(2m-1)}x). \tag{4}$$

A different mode expansion is used to investigate the effect of modes with three longitudinal half-waves,

$$w(x,\theta,t) = \sum_{m=1}^{2} [A_{m,n}(t)\cos(n\theta) + B_{m,n}(t)\sin(n\theta)]\sin(\lambda_{(2m-1)}x) + \sum_{m=1}^{2} A_{(2m-1),0}(t)\sin(\lambda_{(2m-1)}x). \tag{5}$$

Both mode expansions, in equations (4) and (5), have six modes; they allow studying separately the two effects on the harmonic response. Equations (3)–(5) satisfy the boundary conditions

$$w = 0 \quad \text{and} \quad M_x = -D\{(\partial^2 w/\partial x^2) + \nu[\partial^2 w/(R^2\,\partial\theta^2)]\} = 0 \quad \text{at} \quad x = 0, L, \tag{6}$$

where M_x is the bending moment per unit length. The other boundary conditions differ for the simply supported shell of finite length (Case 1) and for the infinitely long, periodically supported shell with restrained axial displacement at the supports (Case 2). They are as follows:

$$\text{Case 1:} \quad N_x = 0 \quad \text{at} \quad x = 0, L \quad \text{and} \quad v = 0 \quad \text{at } x = 0, L, \tag{7a}$$

$$\text{Case 2:} \quad u = 0 \quad \text{at } x = 0, L \quad \text{and} \quad v = 0 \quad \text{at } x = 0, L; \tag{7b}$$

moreover, u, v and w must be continuous in θ. Case 1 corresponds to the classical simply supported shell and Case 2 to a shell with extensions thereof outside (0, L), as discussed in reference [1].

Modes with a number of axial half-waves larger than one can be studied by using a mode expansion retaining axisymmetric terms with $m-2$, m and $m+2$ axial half-waves for an odd value of m (for an even value of m, the axisymmetric terms are: $m-1$, $m+1$ and $m+3$); the truncation effect could be checked also in this case as done for $m = 1$.

3. GALERKIN SOLUTION

The solution of the problem is obtained by a Galerkin projection of the equation of motion (1) when the homogeneous F_h and the particular F_p solutions of the stress function $F = F_h + F_p$ are found. The following two sections present the solution for the two different mode expansions given in equations (4) and (5).

3.1. MODE EXPANSION INCLUDING MODES WITH 2n CIRCUMFERENTIAL WAVES

Substituting the expansion of w, equation (4), in the right-hand side of equation (2), a partial differential equation for the stress function F is obtained. The particular solution is given by

$$\begin{aligned} F_p = {} & [c_1(t)\cos(n\theta) + c_2(t)\sin(n\theta) + c_3(t)\cos(2n\theta) + c_4(t)\sin(2n\theta)]\sin(\pi x/L) \\ & + c_5(t)\sin(\pi x/L) + c_6(t)\sin(3\pi x/L) + c_7(t)\cos(2\pi/L) + c_8(t)\cos(n\theta) \\ & + c_9(t)\cos(n\theta)\cos(2\pi x/L) + c_{10}(t)\cos(n\theta)\cos(4\pi x/L) + c_{11}(t)\sin(n\theta) \\ & + c_{12}(t)\sin(n\theta)\cos(2\pi x/L) + c_{13}(t)\sin(n\theta)\cos(4\pi x/L) + c_{14}(t)\cos(2n\theta) \end{aligned} \tag{8}$$

$$+ c_{15}(t)\cos(2n\theta)\cos(2\pi x/L) + c_{16}(t)\cos(2n\theta)\cos(4\pi x/L) + c_{17}(t)\sin(2n\theta)$$

$$+ c_{18}(t)\sin(2n\theta)\cos(2\pi x/L) + c_{19}(t)\sin(2n\theta)\cos(4\pi x/L) + c_{20}(t)\cos(3n\theta)$$

$$+ c_{21}(t)\cos(3n\theta)\cos(2\pi x/L) + c_{22}(t)\sin(3n\theta) + c_{23}(t)\sin(3n\theta)\cos(2\pi x/L)$$

$$+ c_{24}(t)\cos(4n\theta) + c_{25}(t)\sin(4n\theta),$$

where the functions c_i , $i = 1, \ldots, 25$, are given in Appendix A.

The expansion used for the transverse displacement w satisfies the boundary conditions given by equations (6); moreover, it satisfies exactly the continuity of circumferential displacement, similar to the expansion used in reference [1]. The boundary conditions for either of the in-plane displacements, equations (7), are satisfied "on the average" [1].

The homogeneous solution of equation (2) may be assumed to be of the form [1]

$$F_h = \frac{1}{2}\bar{N}_x R^2\theta^2 + \frac{1}{2}x^2\left\{\bar{N}_\theta + \frac{2Eh}{R\pi}\left[A_{1,0}(t) + \frac{A_{3,0}(t)}{3}\right]\right\} - \bar{N}_{x\theta}xR\theta, \tag{9}$$

where $\bar{N}_x$, $\bar{N}_\theta$ and $\bar{N}_{x\theta}$ are the in-plane restraint stress resultants generated at the ends of the shell, as a consequence of the in-plane constraints on the average. Equation (9) is not the most general homogeneous solution, but it is chosen in order to satisfy the boundary conditions on the average. In fact, it satisfies the forces per unit length in the axial $\bar{N}_x$ and circumferential $\bar{N}_\theta$ directions, as well as the shear force $\bar{N}_{x\theta}$, on the average [1] as a consequence of (i) the contribution of F_p to $\bar{N}_\theta$ being $(2\pi RL)^{-1}\int_0^L\int_0^{2\pi}[\partial^2 F_p/\partial x^2]\,R\mathrm{d}\theta\,\mathrm{d}x$ and (ii) contributions of F_p to $\bar{N}_x$ and $\bar{N}_{x\theta}$ being zero. The boundary conditions allow us to express the in-plane restraint stresses $\bar{N}_x$, $\bar{N}_\theta$ and $\bar{N}_{x\theta}$ [1] in terms of w and its derivatives. For Case 1 they give

$$\bar{N}_x = 0, \tag{10a}$$

$$\bar{N}_\theta = Eh\left\{-\frac{2}{\pi R}\left[A_{1,0}(t) + \frac{A_{3,0}(t)}{3}\right] + \frac{n^2}{8R^2}\left[A_{1,n}^2(t) + B_{1,n}^2(t) + 4A_{1,2n}^2(t) + 4B_{1,2n}^2(t)\right]\right\}, \tag{11a}$$

$$\bar{N}_{x\theta} = 0; \tag{12a}$$

while for Case 2, they give

$$\bar{N}_x = \frac{Eh}{1-\nu^2}\left\{-2\nu\left[\frac{1}{\pi R}\left[A_{1,0}(t) + \frac{A_{3,0}(t)}{3}\right] + \frac{\pi^2}{4L^2}\left[A_{1,0}^2(t) + 9A_{3,0}^2(t)\right]\right.\right.$$

$$+ \frac{\pi^2}{8L^2}\left[A_{1,n}^2(t) + B_{1,n}^2(t) + A_{1,2n}^2(t) + B_{1,2n}^2(t)\right] \tag{10b}$$

$$\left.\left. + \frac{\nu n^2}{8R^2}\left[A_{1,n}^2(t) + B_{1,n}^2(t) + 4A_{1,2n}^2(t) + 4B_{1,2n}^2(t)\right]\right\},$$

$$\bar{N}_\theta = \frac{Eh}{1-\nu^2}\left\{\frac{-2}{\pi R}\left[A_{1,0}(t)+\frac{A_{3,0}(t)}{3}\right]+\frac{\nu\pi^2}{4L^2}[A_{1,0}^2(t)+9A_{3,0}^2(t)]\right.$$

$$+\frac{\nu\pi^2}{8L^2}[A_{1,n}^2(t)+B_{1,n}^2(t)+A_{1,2n}^2(t)+B_{1,2n}^2(t)] \tag{11b}$$

$$\left.+\frac{n^2}{8R^2}[A_{1,n}^2(t)+B_{1,n}^2(t)+4A_{1,2n}^2(t)+4B_{1,2n}^2(t)]\right\},$$

$$\bar{N}_{x\theta} = 0. \tag{12b}$$

3.2. MODE EXPANSION INCLUDING MODES WITH THREE LONGITUDINAL HALF-WAVES

Substituting the expansion of w, equation (5), into the right-hand side of equation (2), a partial differential equation for the stress function F is obtained. The particular solution is given by

$$\begin{aligned}F_p = {} & [c_1(t)\cos(n\theta)+c_2(t)\sin(n\theta)]\sin(\pi x/L)+[c_3(t)\cos(n\theta)+c_4(t)\sin(n\theta)]\sin(3\pi x/L)\\ & +c_5(t)\sin(\pi x/L)+c_6(t)\sin(3\pi x/L)+c_7(t)\cos(2\pi x/L)+c_8(t)\cos(4\pi x/L)\\ & +c_9(t)\cos(6\pi x/L)+c_{10}(t)\cos(n\theta)+c_{11}(t)\cos(n\theta)\cos(2\pi x/L)\\ & +c_{12}(t)\cos(n\theta)\cos(4\pi x/L)+c_{13}(t)\cos(n\theta)\cos(6\pi x/L)+c_{14}(t)\sin(n\theta)\\ & +c_{15}(t)\sin(n\theta)\cos(2\pi x/L)+c_{16}(t)\sin(n\theta)\cos(4\pi x/L)+c_{17}(t)\sin(n\theta)\cos(6\pi x/L)\\ & +c_{18}(t)\cos(2n\theta)+c_{19}(t)\cos(2n\theta)\cos(2\pi x/L)+c_{20}(t)\cos(2n\theta)\cos(4\pi x/L)\\ & +c_{21}(t)\sin(2n\theta)+c_{22}(t)\sin(2n\theta)\cos(2\pi x/L)+c_{23}(t)\sin(2n\theta)\cos(4\pi x/L),\end{aligned} \tag{13}$$

where the functions c_i , $i = 1, \ldots, 23$, are given in Appendix B.

Equation (5) satisfies the boundary conditions given by equations (6); moreover, it satisfies exactly the continuity of circumferential displacement. The boundary conditions for either of the in-plane displacements, equations (7), are satisfied "on the average".

The homogeneous solution is still given by equation (9). The stress resultants $\bar{N}_x$, $\bar{N}_\theta$ and $\bar{N}_{x\theta}$ are given by

$$\bar{N}_x = 0, \tag{14a}$$

$$\bar{N}_\theta = Eh\left\{-\frac{2}{\pi R}\left[A_{1,0}(t)+\frac{A_{3,0}(t)}{3}\right]\right.$$

$$\left.+\frac{n^2}{8R^2}[A_{1,n}^2(t)+B_{1,n}^2(t)+A_{3,n}^2(t)+B_{3,n}^2(t)]\right\}, \tag{15a}$$

$$\bar{N}_{x\theta} = 0; \tag{16a}$$

while for Case 2, they give

$$\bar{N}_x = \frac{Eh}{1-\nu^2}\left\{\frac{-2\nu}{\pi R}\left[A_{1,0}(t) + \frac{A_{3,0}(t)}{3}\right] + \frac{\pi^2}{4L^2}\left[A_{1,0}^2(t) + 9A_{3,0}^2(t)\right]\right.$$

$$+ \frac{\pi^2}{8L^2}\left[A_{1,n}^2(t) + B_{1,n}^2(t) + 9A_{3,n}^2(t) + 9B_{3,n}^2(t)\right]$$

$$\left. + \frac{\nu n^2}{8R^2}\left[A_{1,n}^2(t) + B_{1,n}^2(t) + A_{3,n}^2(t) + B_{3,n}^2(t)\right]\right\}, \tag{14b}$$

$$\bar{N}_\theta = \frac{Eh}{1-\nu^2}\left\{\frac{-2}{\pi R}\left[A_{1,0}(t) + \frac{A_{3,0}(t)}{3}\right] + \frac{\nu\pi^2}{4L^2}\left[A_{1,0}^2(t) + 9A_{3,0}^2(t)\right]\right.$$

$$+ \frac{\nu\pi^2}{8L^2}\left[A_{1,n}^2(t) + B_{1,n}^2(t) + 9A_{3,n}^2(t) + 9B_{3,n}^2(t)\right]$$

$$\left. + \frac{n^2}{8R^2}\left[A_{1,n}^2(t) + B_{1,n}^2(t) + A_{3,n}^2(t) + B_{3,n}^2(t)\right]\right\}, \tag{15b}$$

$$\bar{N}_{x\theta} = 0. \tag{16b}$$

3.3. GALERKIN PROJECTION AND EQUATIONS OF MOTION

By using the Galerkin method, six second order ordinary, coupled non-linear differential equations are obtained for the variables $A_{1,n}(t)$, $B_{1,n}(t)$, $A_{1,2n}(t)$ or $A_{3,n}(t)$, $B_{1,2n}(t)$ or $B_{3,n}(t)$, $A_{1,0}(t)$ and $A_{3,0}(t)$, by successively weighting the single original equation with the weighting functions z_s and integrating over the shell middle surface. The weighting functions z_s are defined as

$$z_s(x,\theta) = \begin{cases} \cos(n\theta)\sin(\pi x/L) & \text{for } s = 1, \\ \sin(n\theta)\sin(\pi x/L) & \text{for } s = 2, \\ \cos(2n\theta)\sin(\pi x/L) \text{ or } \cos(n\theta)\sin(3\pi x/L) & \text{for } s = 3, \\ \sin(2n\theta)\sin(\pi x/L) \text{ or } \sin(n\theta)\sin(3\pi x/L) & \text{for } s = 4, \\ \sin(\pi x/L) & \text{for } s = 5, \\ \sin(3\pi x/L) & \text{for } s = 6. \end{cases} \tag{17}$$

The Galerkin projection of the equation of motion (1) has been performed by using the *Mathematica* computer software [8]. The modal excitation $f = f_n\cos(n\theta)\sin(\pi x/L)\cos(\omega t)$ is considered. In particular, for the mode expansion including modes with $2n$ circumferential waves and axial constraint $N_x = 0$ at $x = 0$, L, the following system of six equations is obtained. The first one is

$$\ddot{A}_{1,n}(t) + 2\zeta_{1,n}\omega_{1,n}\dot{A}_{1,n}(t) + \omega_{1,n}^2 A_{1,n}(t) + h_1 A_{1,n}^3(t) + h_1 A_{1,n}(t)B_{1,n}^2(t) + h_2 A_{1,n}(t)A_{1,2n}(t)$$

$$+ h_2 B_{1,n}(t)B_{1,2n}(t) + h_3 A_{1,n}(t)A_{1,2n}^2(t) + h_3 A_{1,n}(t)B_{1,2n}^2(t) + h_4 A_{1,n}(t)A_{1,0}(t)$$

$$+ h_5 A_{1,n}(t) A_{3,0}(t) + h_6 A_{1,n}(t) A_{1,0}^2(t) + h_7 A_{1,n}(t) A_{3,0}^2(t) + h_8 A_{1,n}(t) A_{1,2n}(t) A_{1,0}(t)$$

$$+ h_8 B_{1,n}(t) B_{1,2n}(t) A_{1,0}(t) + h_9 A_{1,n}(t) A_{1,2n}(t) A_{3,0}(t) + h_9 B_{1,n}(t) B_{1,2n}(t) A_{3,0}(t)$$

$$+ h_{10} A_{1,n}(t) A_{1,0}(t) A_{3,0}(t) = \frac{\pi L f_n}{2m_1} \cos(\omega t), \tag{18a}$$

where

$$m_1 = \rho h \pi L/2 + \rho_F L^2 \mathrm{I}_n(\pi R/L)/[2I_n'(\pi R/L)],$$

$$\omega_{1,n}^2 = \frac{\pi L}{2}\left[D\left(\frac{\pi^2}{L^2} + \frac{n^2}{R^2}\right)^2 + \frac{Eh\pi^4}{R^2 L^4}\Big/\left(\frac{\pi^2}{L^2} + \frac{n^2}{R^2}\right)^2 \right]\Big/ m_1, \quad \zeta_{1,n} = ch\frac{\pi L}{2}\Big/(2\omega_{1,n} m_1),$$

and h_i, $i = 1, \ldots, 10$, are coefficients depending on geometry, material properties and n that arise from projections of the part of equation (1) involving the stress function F. The second equation has the same form as equation (18a) without excitation, but with $A_{1,n}$ replaced by $B_{1,n}$ and *vice versa*,

$$\ddot{B}_{1,n}(t) + 2\zeta_{1,n}\omega_{1,n}\dot{B}_{1,n}(t) + \omega_{1,n}^2 B_{1,n}(t) + h_1 B_{1,n}^3(t) + h_1 B_{1,n}(t) A_{1,n}^2(t) + h_2 B_{1,n}(t) A_{1,2n}(t)$$

$$+ h_2 A_{1,n}(t) B_{1,2n}(t) + h_3 B_{1,n}(t) A_{1,2n}^2(t) + h_3 B_{1,n}(t) B_{1,2n}^2(t) + h_4 B_{1,n}(t) A_{1,0}(t)$$

$$+ h_5 B_{1,n}(t) A_{3,0}(t) + h_6 B_{1,n}(t) A_{1,0}^2(t) + h_7 B_{1,n}(t) A_{3,0}^2(t) + h_8 B_{1,n}(t) A_{1,2n}(t) A_{1,0}(t)$$

$$+ h_8 A_{1,n}(t) B_{1,2n}(t) A_{1,0}(t) + h_9 B_{1,n}(t) A_{1,2n}(t) A_{3,0}(t) + h_9 A_{1,n}(t) B_{1,2n}(t) A_{3,0}(t)$$

$$+ h_{10} B_{1,n}(t) A_{1,0}(t) A_{3,0}(t) = 0. \tag{18b}$$

The third equation is

$$\ddot{A}_{1,2n}(t) + 2\zeta_{1,2n}\omega_{1,2n}\dot{A}_{1,2n}(t) + \omega_{1,2n}^2 A_{1,2n}(t) + k_1 A_{1,2n}^3(t) + k_1 A_{1,2n}(t) B_{1,2n}^2(t)$$

$$+ k_2 A_{1,2n}(t) A_{1,n}^2(t) + k_2 A_{1,2n}(t) B_{1,n}^2(t) + k_3 A_{1,2n}(t) A_{1,0}(t) + k_4 A_{1,2n}(t) A_{3,0}(t)$$

$$+ k_5 A_{1,2n}(t) A_{1,0}^2(t) + k_6 A_{1,2n}(t) A_{3,0}^2(t) + k_7 A_{1,2n}(t) A_{1,0}(t) A_{3,0}(t) + k_8 A_{1,n}^2(t)$$

$$- k_8 B_{1,n}^2(t) - k_9 A_{1,n}^2(t) A_{1,0}(t) + k_9 B_{1,n}^2(t) A_{1,0}(t)$$

$$+ k_{10} A_{1,n}^2(t) A_{3,0}(t) - k_{10} B_{1,n}^2(t) A_{3,0}(t) = 0, \tag{18c}$$

where

$$m_2 = \rho h \pi L/2 + \rho_F L^2 \mathrm{I}_{2n}(\pi R/L)/[2\mathrm{I}_{2n}'(\pi R/L)],$$

$$\omega_{1,2n}^2 = \frac{\pi L}{2}\left[D\left(\frac{\pi^2}{L^2} + \frac{4n^2}{R^2}\right)^2 + \frac{Eh\pi^4}{R^2 L^4}\Big/\left(\frac{\pi^2}{L^2} + \frac{4n^2}{R^2}\right)^2 \right]\Big/ m_2, \quad \zeta_{1,2n} = ch\frac{\pi L}{2}\Big/(2\omega_{1,2n} m_2),$$

and k_i, $i = 1, \ldots, 10$, are appropriate coefficients. The fourth equation is

$$\ddot{B}_{1,2n}(t) + 2\zeta_{1,2n}\omega_{1,2n}\dot{B}_{1,2n}(t) + \omega_{1,2n}^2 B_{1,2n}(t) + k_1 B_{1,2n}^3(t) + k_1 B_{1,2n}(t) A_{1,2n}^2(t)$$
$$+ k_2 B_{1,2n}(t) A_{1,n}^2(t) + k_2 B_{1,2n}(t) B_{1,n}^2(t) + k_3 B_{1,2n}(t) A_{1,0}(t) + k_4 B_{1,2n}(t) A_{3,0}(t)$$
$$+ k_5 B_{1,2n}(t) A_{1,0}^2(t) + k_6 B_{1,2n}(t) A_{3,0}^2(t) + k_7 B_{1,2n}(t) A_{1,0}(t) A_{3,0}(t)$$
$$+ 2k_8 A_{1,n}(t) B_{1,n}(t) - 2k_9 A_{1,n}(t) B_{1,n}(t) A_{1,0}(t) + 2k_{10} A_{1,n}(t) B_{1,n}(t) A_{3,0}(t) = 0. \quad (18d)$$

The fifth equation, that is related to the first axisymmetric d.o.f., is given by

$$\ddot{A}_{1,0}(t) + 2\zeta_{1,0}\omega_{1,0}\dot{A}_{1,0}(t) + \omega_{1,0}^2 A_{1,0}(t) + l_1 A_{1,0}(t) A_{1,n}^2(t) + l_1 A_{1,0}(t) B_{1,n}^2(t)$$
$$+ l_2 A_{1,0}(t) A_{1,2n}^2(t) + l_2 A_{1,0}(t) B_{1,2n}^2(t) + l_3 A_{1,n}^2(t) + l_3 B_{1,n}^2(t) + l_4 A_{1,2n}^2(t) + l_4 B_{1,2n}^2(t)$$
$$+ l_5 A_{3,0}(t) A_{1,n}^2(t) + l_5 A_{3,0}(t) B_{1,n}^2(t) + l_6 A_{3,0}(t) A_{1,2n}^2(t) + l_6 A_{3,0}(t) B_{1,2n}^2(t)$$
$$+ l_7 A_{1,2n}(t) B_{1,n}^2(t) - l_7 A_{1,2n}(t) A_{1,n}^2(t) - 2l_7 B_{1,2n}(t) A_{1,n}(t) B_{1,n}(t) = 0, \quad (18e)$$

where

$$m_{1,0} = \rho h \pi L + \rho_F L^2 \mathrm{I}_0(\pi R/L)/\mathrm{I}_0'(\pi R/L),$$
$$\omega_{1,0}^2 = \frac{\pi L}{m_{1,0}}\left(\frac{D\pi^4}{L^4} + \frac{Eh}{R^2}\right), \quad \zeta_{1,0} = ch\pi L/(2\omega_{1,0} m_{1,0}),$$

and l_i, $i = 1, \ldots, 7$, are appropriate coefficients. The sixth equation is

$$\ddot{A}_{3,0}(t) + 2\zeta_{3,0}\omega_{3,0}\dot{A}_{3,0}(t) + \omega_{3,0}^2 A_{3,0}(t) + n_1 A_{3,0}(t) A_{1,n}^2(t) + n_1 A_{3,0}(t) B_{1,n}^2(t)$$
$$+ n_2 A_{3,0}(t) A_{1,2n}^2(t) + n_2 A_{3,0}(t) B_{1,2n}^2(t) + n_3 A_{1,n}^2(t) + n_3 B_{1,n}^2(t) + n_4 A_{1,2n}^2(t)$$
$$+ n_4 B_{1,2n}^2(t) + n_5 A_{1,0}(t) A_{1,n}^2(t) + n_5 A_{1,0}(t) B_{1,n}^2(t) + n_6 A_{1,0}(t) A_{1,2n}^2(t)$$
$$+ n_6 A_{1,0}(t) B_{1,2n}^2(t) + n_7 A_{1,2n}(t) A_{1,n}^2(t) - n_7 A_{1,2n}(t) B_{1,n}^2(t)$$
$$+ 2n_7 B_{1,2n}(t) A_{1,n}(t) B_{1,n}(t) = 0, \quad (18f)$$

where

$$m_{3,0} = \rho h \pi L + \rho_F L^2 \mathrm{I}_0(3\pi R/L)/[3\mathrm{I}_0'(3\pi R/L)],$$
$$\omega_{3,0}^2 = \frac{\pi L}{m_{3,0}}\left(\frac{81D\pi^4}{L^4} + \frac{Eh}{R^2}\right), \quad \zeta_{3,0} = ch\pi L/(2\omega_{3,0} m_{3,0}),$$

and n_i, $i = 1, \ldots, 7$, are appropriate coefficients.

4. NUMERICAL RESULTS

Numerical computations have been carried out for both empty and water-filled shells, for the same cases already investigated in Parts I and II [1, 2] of the present study.

4.1. SHELL *IN VACUO*

The case analyzed here was initially studied by Chen and Babcock [7] and was also studied by Amabili *et al.* [2, 4]. It relates to a circular cylindrical shell in vacuum, simply supported at the ends (with zero axial force N_x), and having the following dimensions and properties: $L = 0{\cdot}2$ m, $R = 0{\cdot}1$ m, $h = 0{\cdot}247 \times 10^{-3}$ m, $E = 71{\cdot}02 \times 10^9$ Pa, $\rho = 2796$ kg/m^3 and $\nu = 0{\cdot}31$; the mode investigated is $n = 6$ and $m = 1$. The amplitude of the external modal excitation is $f_{1,n} = 0{\cdot}0012h^2\rho\omega_{1,n}^2$, and the damping ratio $\zeta_{1,n} = 0{\cdot}0005$ (with $\zeta_{1,2n} = \zeta_{1,n}\omega_{1,2n}/\omega_{1,n}$, $\zeta_{3,n} = \zeta_{1,n}\omega_{3,n}/\omega_{1,n}$, $\zeta_{1,0} = \zeta_{1,n}\omega_{1,0}/\omega_{1,n}$ and $\zeta_{3,0} = \zeta_{1,n}\omega_{3,0}/\omega_{1,n}$); the linear radian frequencies are $\omega_{1,n} = 2\pi \times 564{\cdot}2$ rad/s, $\omega_{1,2n} = 2\pi \times 891{\cdot}8$ rad/s, $\omega_{3,n} = 2\pi \times 3080$ rad/s, $\omega_{1,0} = 2\pi \times 8021$ rad/s, $\omega_{3,0} = 2\pi \times 8023$ rad/s. All the numerical results have been obtained by using the software *AUTO* [9] for bifurcation and continuation of the solution of ordinary differential equations, based on a collocation method. The periodic solutions obtained show the maximum amplitude of the generalized co-ordinates in a period.

Figure 1 shows the frequency–response relationship of the driven mode, without companion mode participation, when the excitation frequency is in the neighbourhood of the linear resonance of mode (1, 6), computed by using mode expansions including driven and companion modes, in addition to: (i) two asymmetric modes with $2n$ circumferential waves plus two axisymmetric modes (thick continuous line); (ii) three axisymmetric modes (thin continuous line); (iii) two axisymmetric modes (dashed line); and (iv) only the first

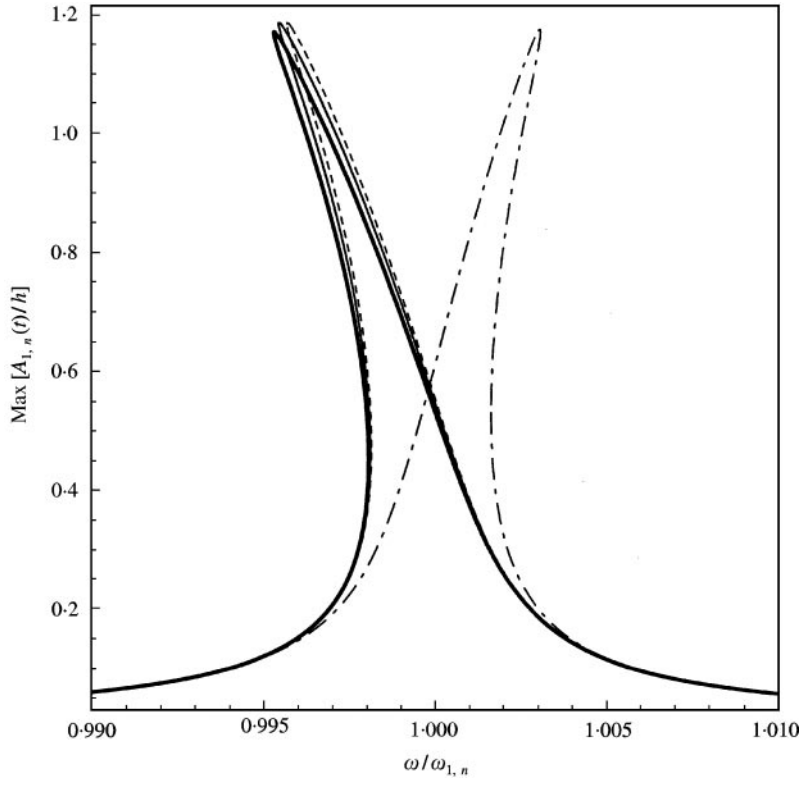

Figure 1. Frequency–response curves for the driven mode without companion mode participation, $m = 1$: ——, model including modes with $2n$ circumferential waves; ——, model with three axisymmetric modes; — — —, model with two axisymmetric modes; ·-·-·-·, model with one axisymmetric mode.

axisymmetric mode (chain-dotted line). The axisymmetric modes considered have an odd number of longitudinal half-waves, for the reasons discussed in reference [2]. The curves corresponding to cases (ii)–(iv) are given in Figure 2 of reference [2] and are reported here only for comparison. The response obtained with the asymmetric modes having three longitudinal half-waves plus two axisymmetric modes overlaps perfectly the curve of case (iii), i.e., with two axisymmetric modes only. It means that the effect of additional longitudinal modes is absolutely negligible in the single-mode response without fluid flow. It is very interesting to observe that the curves corresponding to cases (i) and (iii) are quite close, i.e., the effect of modes with $2n$ circumferential waves is limited, so far as the single-mode response of the shell is concerned.

As a consequence of the insensitivity of the response to additional asymmetric modes as compared to computations with only the driven and the axisymmetric modes, it is reasonably believed that further increases in the number of asymmetric modes would not significantly change the single-mode response of this shell.

Figure 2 shows the frequency–response relationship with companion mode participation for the model including modes with $2n$ circumferential waves. When this figure is compared to Figure 3 of reference [2], it becomes evident that the response with companion mode participation is significantly affected by modes with $2n$ circumferential waves. In fact, the companion mode response $B_{1,n}(t)$ participates over an enlarged frequency range. The stable area in branch 2 at the tip of the response $A_{1,n}(t)$ is decreased and there is a second peak at the right-hand end of branch 2. Moreover, the response $A_{1,n}(t)$ in branch 2 is diminished; this means that travelling wave response develops at smaller vibration amplitudes. Another interesting phenomenon is that no stable solutions exist for $0{\cdot}9981 < \omega/\omega_{1,n} < 0{\cdot}9998$ (the non-existence of stable solutions simply means that no stable *periodic* solutions exist). For the same case, neglecting modes with $2n$ circumferential waves, no regions without stable solutions are obtained [2]. A further complication is shown in Figure 2(d), relating to $B_{1,2n}(t)$, where a third branch appears. Bifurcations of branch "1" are of the pitchfork type; the loss of stability of branch "2" is due to foldings in the phase diagrams (with respect to the excitation); these conclusions can be proved with a perturbation analysis, as performed in reference [4].

Figure 3 shows the frequency–response relationship with companion mode participation for the model including modes with three longitudinal half-waves. This figure is the same as that obtained neglecting modes with three longitudinal half-waves [2], except for Figures 3(c, d) that show the maximum amplitude of $A_{3,n}(t)$ and $B_{3,n}(t)$. The amplitudes of these generalized co-ordinates are at least one order of magnitude lower than that of the first axisymmetric mode $A_{1,0}(t)$. No additional branches have been detected in this case.

It has been observed in Figure 2 that no stable periodic solutions exist for $0{\cdot}9981 < \omega/\omega_{1,n} < 0{\cdot}9998$, for the model including modes with $2n$ circumferential waves. Therefore, the response of the system to harmonic excitation has been investigated further in this region. The Poincaré maps obtained for the six generalized co-ordinates for $\omega/\omega_{1,n} = 0{\cdot}999$ are given in Figure 4 and show a limit cycle; the Poincaré maps have been obtained by direct integration of the equations of motion, performed by using an adaptive step-size Runge–Kutta integration scheme; the maps are obtained by using the points computed at the instant where the amplitude of the force is maximum. The limit cycle is an attractive one-dimensional set embedded in a 12-D phase space in the Poincaré map. The limit cycle shows a modulated harmonic response, as can be observed in Figure 5(a), which shows the time response $A_{1,n}(t)$. This figure also shows that the maximum of $A_{1,n}(t)$ in any excitation period is approximately comprised between the two unstable branches "1" and "2" for $\omega/\omega_{1,n} = 0{\cdot}999$ (see Figure 2(a)). The response is not chaotic as can be ascertained

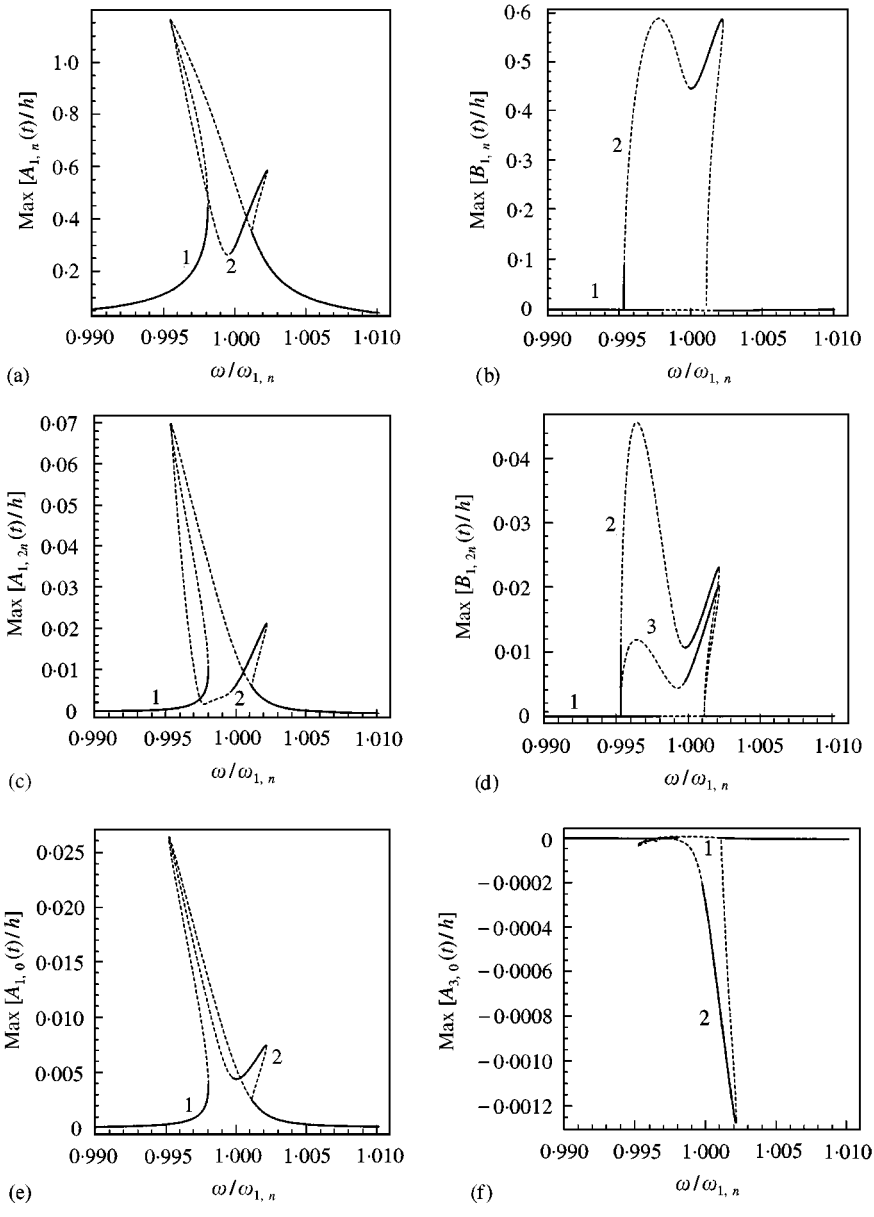

Figure 2. Frequency–response curve with companion mode participation for the model including modes with $2n$ circumferential waves. (a) Maximum of $A_{1,n}(t)/h$; (b) maximum of $B_{1,n}(t)/h$; (c) maximum of $A_{1,2n}(t)/h$; (d) maximum of $B_{1,2n}(t)/h$; (e) maximum of $A_{1,0}(t)/h$; (f) maximum of $A_{3,0}(t)/h$. ——, Stable solutions; — — —, unstable solutions.

from the frequency spectrum given in Figure 5(b). It shows that the single frequency response obtained in the stable region is divided into several closely spaced frequencies that give a beating phenomenon. The whole area where no stable solutions exist is associated with beating phenomena that give modulations in the oscillation amplitude. Note that the small portion of the spectrum given in Figure 5(b) contains most of the energy in the time signal, i.e., no harmonic components are present at lower and higher frequencies.

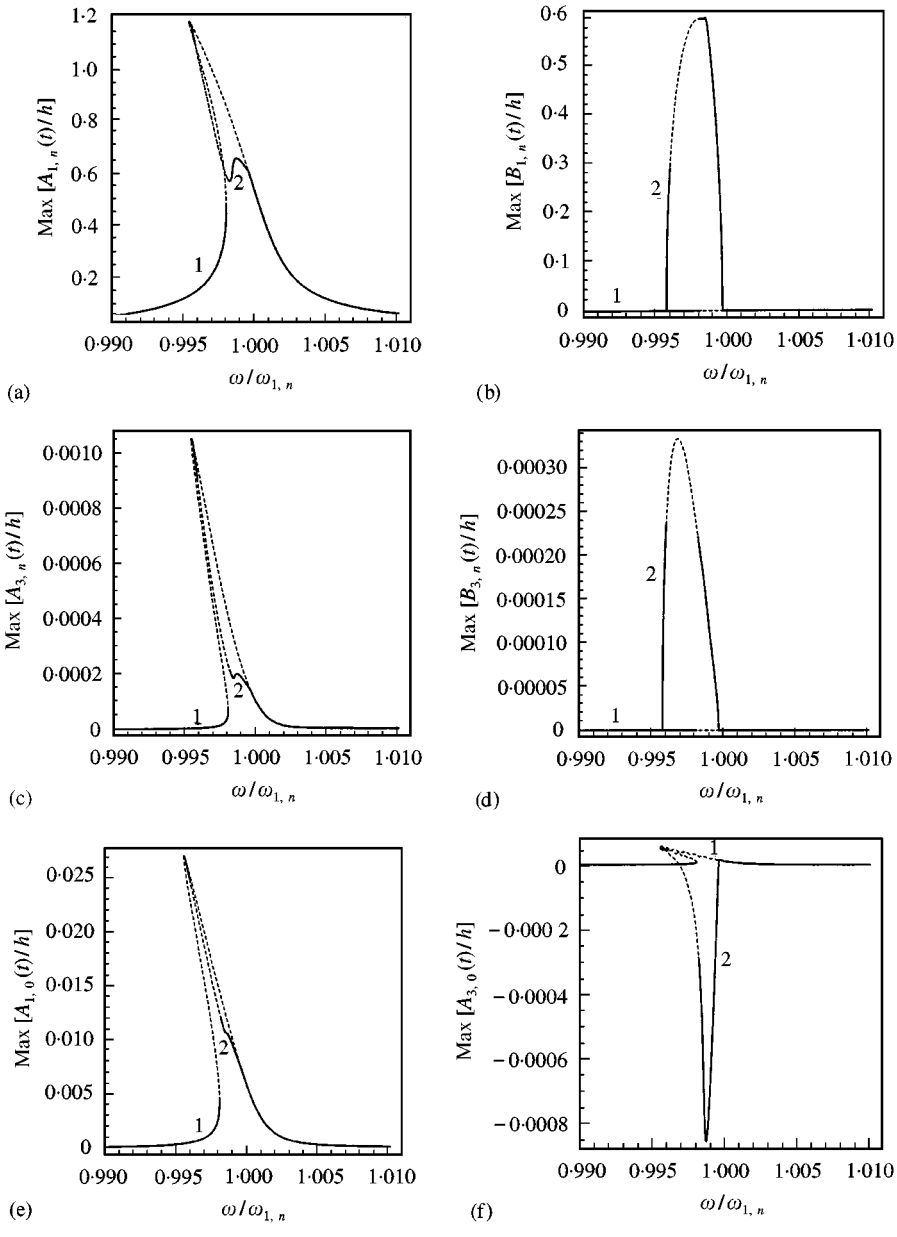

Figure 3. Frequency–response curve with companion mode participation for the model including modes with three longitudinal half-waves. (a) Maximum of $A_{1,n}(t)/h$; (b) maximum of $B_{1,n}(t)/h$; (c) maximum of $A_{3,n}(t)/h$; (d) maximum of $B_{3,n}(t)/h$; (e) maximum of $A_{1,0}(t)/h$; (f) maximum of $A_{3,0}(t)/h$. ——, Stable solutions; — — —, unstable solutions.

4.2. WATER-FILLED SHELL

A case presenting a much stronger non-linearity is a water-filled circular cylindrical shell, simply supported at the ends ($N_x = 0$), with the following characteristics: $L/R = 2$, $h/R = 0{\cdot}01$, $E = 206 \times 10^9$ Pa, $\rho = 7850\ \text{kg/m}^3$, $\rho_F = 1000\ \text{kg/m}^3$ and $\nu = 0{\cdot}3$ previously studied in references [1, 2]. In this case, no fluid flow is considered, the shell ends are open

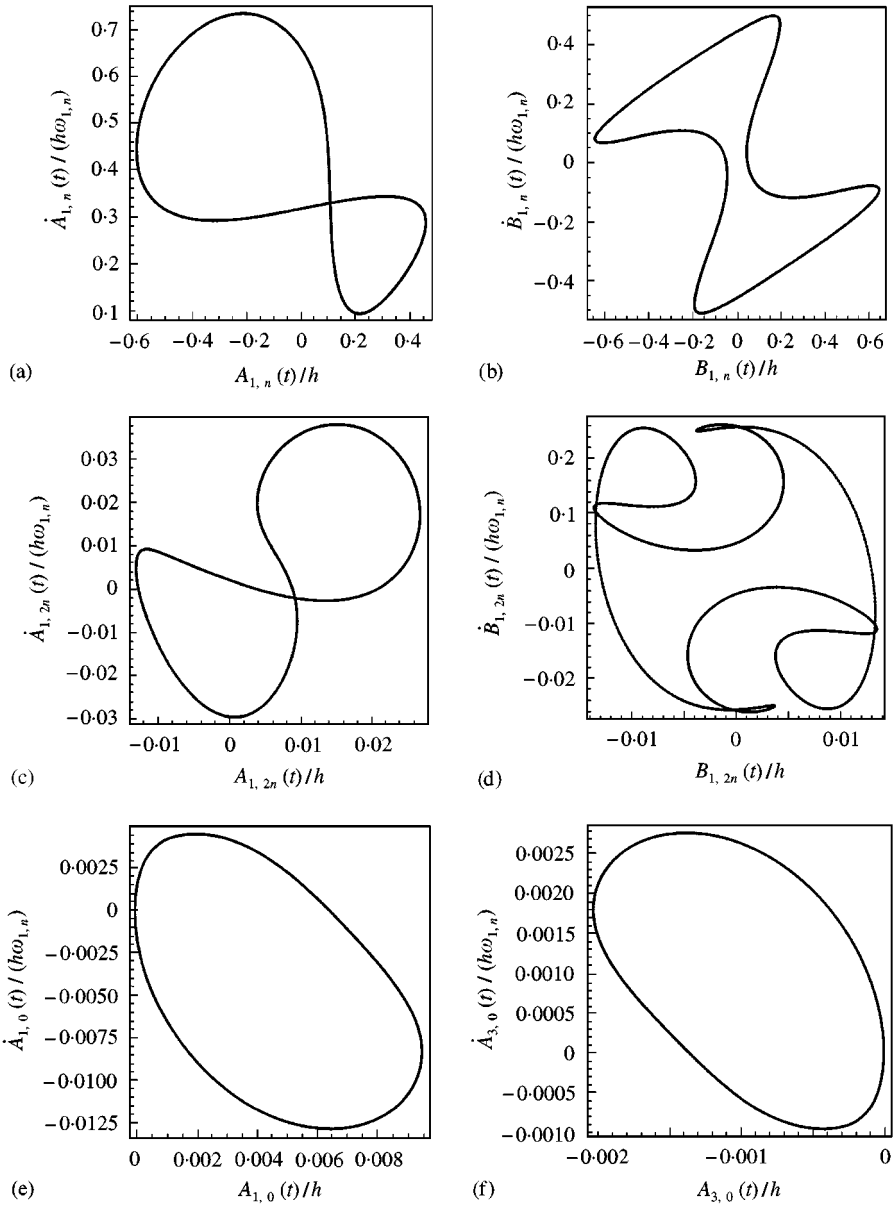

Figure 4. Poincaré maps for $\omega/\omega_{1,n} = 0{\cdot}999$ and $f_{1,n} = 0{\cdot}0012h^2\rho\omega_{1,n}^2$ showing limit-cycle motion. (a) First generalized co-ordinate; (b) second generalized co-ordinate; (c) third generalized co-ordinate; (d) fourth generalized co-ordinate; (e) fifth generalized co-ordinate; (f) sixth generalized co-ordinate.

(zero pressure at $x = 0, L$) and a linear fluid structure-interaction model has been used. The mode considered is $n = 5, m = 1$, with a damping ratio $\zeta_{1,n} = 0{\cdot}01$, a linear radian frequency $\omega_{1,n} = 2\pi \times 106{\cdot}69$ rad/s and an amplitude of the external modal excitation $f_{1,n} = 0{\cdot}03h\omega_{1,n}^2 m_1[2/(\pi L)]$. Only the model including modes with $2n$ circumferential waves is discussed here, since it has been found that additional longitudinal half-waves have a negligible effect.

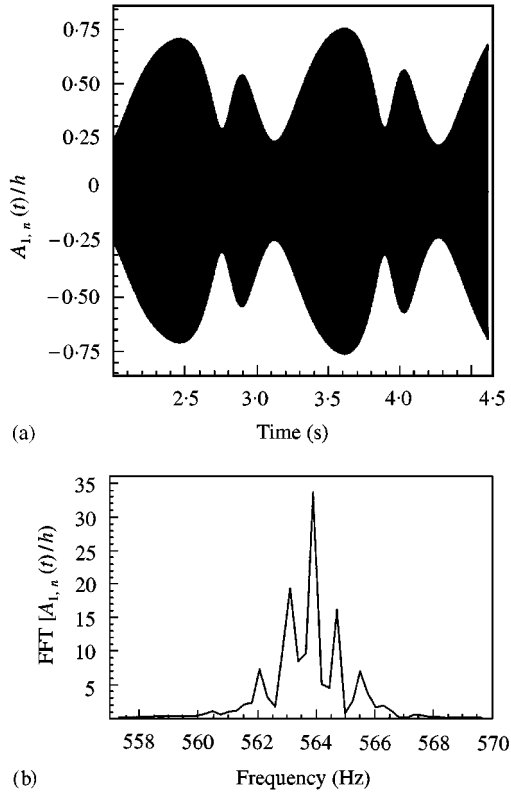

Figure 5. Limit cycle response; $\omega/\omega_{1,n} = 0{\cdot}999$ and $f_{1,n} = 0{\cdot}0012h^2\rho\omega_{1,n}^2$. (a) Time history; (b) frequency spectrum.

The frequency–response relationship with companion mode participation is given in Figure 6. From both the numerical and the qualitative points of view, the response of the system is very close to that obtained in reference [2], where modes with $2n$ circumferential waves were not considered. In particular, a slightly enhanced softening behaviour is observed with respect to the results obtained in reference [2] and additionally branch "3" is observed in the response of the generalized co-ordinate $B_{1,2n}(t)$. Therefore, it is possible to say that, in this case, the modal interaction between the six generalized co-ordinates is significantly reduced with respect to the case *in vacuo* studied in the previous section. This is attributed to the increased damping. As a consequence, the difference between the model presented in references [1, 2] and the present results is negligible in the case of the water-filled shell studied.

5. EXPERIMENTAL RESULTS AND COMPARISON

Tests were conducted on a commercial circular cylindrical tank made of steel and having a longitudinal seam weld. The flat, steel end-plates of the tank were mostly removed, leaving only an annular part, 15 mm wide, to approximate the simply supported boundary condition of the shell; rubber disks 1 mm thick were glued to these annular end-plates. The tank was filled with water. The open-end fluid boundary condition is well approximated by

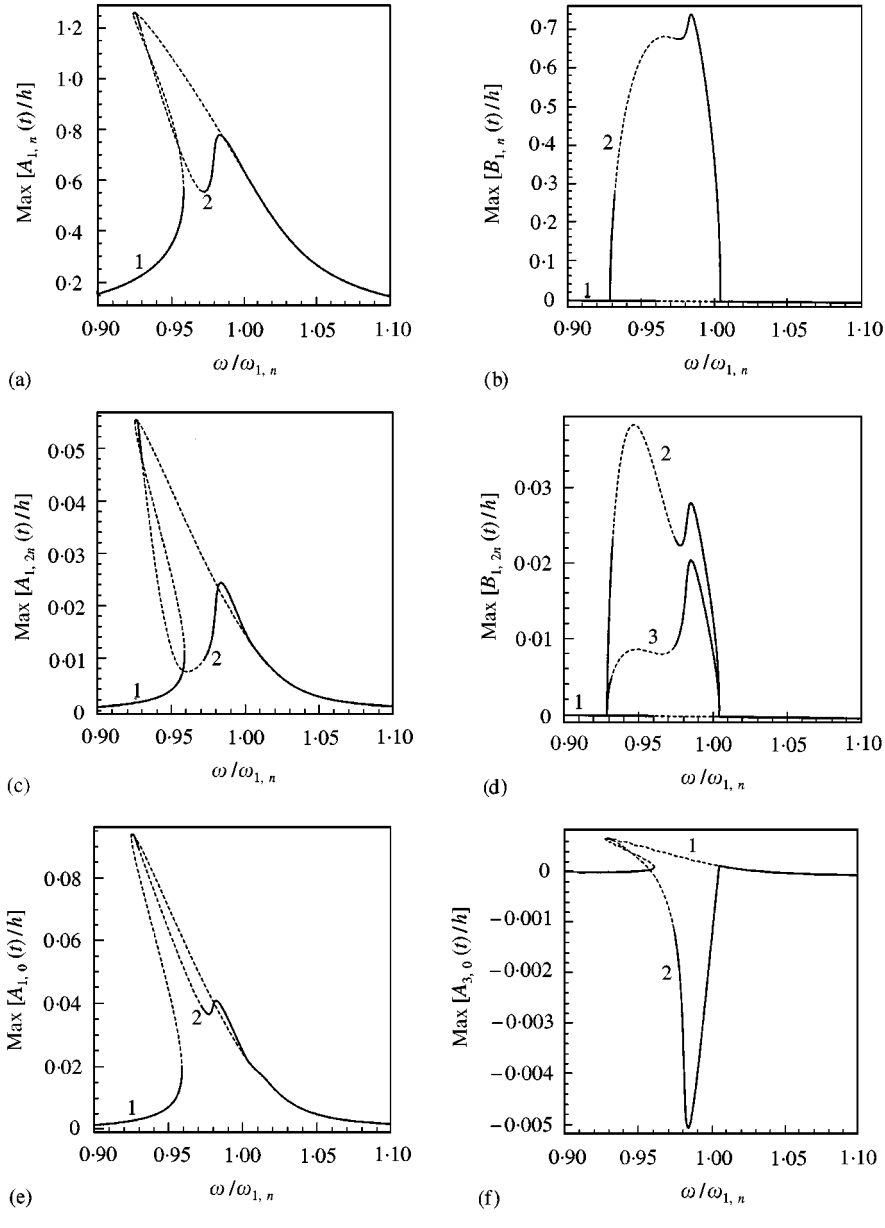

Figure 6. Frequency-response curve with companion mode participation for the model including modes with $2n$ circumferential waves; water-filled shell. (a) Maximum of $A_{1,n}(t)/h$; (b) maximum of $B_{1,n}(t)/h$; (c) maximum of $A_{1,2n}(t)/h$; (d) maximum of $B_{1,2n}(t)/h$; (e) maximum of $A_{1,0}(t)/h$; (f) maximum of $A_{3,0}(t)/h$. ——, Stable solutions; — — —, unstable solutions.

the flexible rubber disks at the shell ends. The dimensions and material properties of the system are: $L = 246$ mm, $R = 86{\cdot}5$ mm, $h = 0{\cdot}23$ mm, $E = 1{\cdot}9 \times 10^{11}$ Pa, $\rho = 7850$ kg/m^3, $\rho_F = 1000$ kg/m^3 and $\nu = 0{\cdot}3$. The shell was suspended with elastic cables to a box-type frame. A picture of the test-shell is given in Figure 7.

The shell was subjected to harmonic excitation in the spectral neighbourhood of the lowest natural frequency, corresponding to mode $n = 6$ and $m = 1$, and its response was

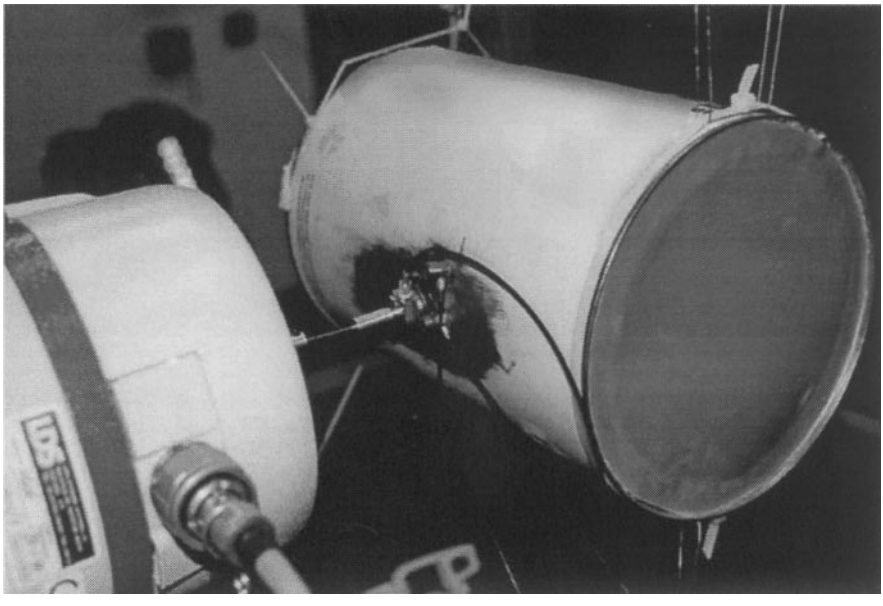

Figure 7. Picture of the tested shell being excited by the shaker.

investigated. The excitation was provided by an electrodynamic exciter (shaker), model LDS V406 with power amplifier LDS PA100E, connected to the shell by a stinger at $x = 0{\cdot}118$ m, i.e., close to $x = L/2$. A piezoelectric force transducer, model B&K 8200, of mass 21 g, was screwed to a base of 3·5 g which was glued to the shell; the stinger was screwed to the force transducer to measure the force transmitted. The shell response was measured by using two accelerometers, model B&K 4393, of mass 2·4 g, glued to the shell at $x = 0{\cdot}096$ mm, i.e., $0{\cdot}39\,L$ ($\sin(\pi x/L) = 0{\cdot}94$). The first accelerometer was placed at the same angular position as the stinger, to measure the driven mode (with a very small contribution of axisymmetric and $\cos(2n\theta)$ terms) and the second one at the same axial location with an angular distance of $\pi/12$, to capture the companion mode. The time responses were measured by using a Difa Scadas II front-end connected to an HP 715/80 workstation and the software Ideas Test for signal processing and data analysis; the same front-end was used to generate the harmonic signal.

The fundamental frequency of the water-filled shell was measured to be 130·9 Hz whereas the theoretical value is 134·7 Hz. The difference is attributed to imperfections in the test specimen and mainly to the added mass due to the sensors glued to the shell. Theoretical and measured natural frequencies are reported in Table 1. The effect of sensors has been

TABLE 1

Theoretical and experimental natural frequencies for the water-filled test-shell

Mode	Theoretical frequency (Hz)	Experimental frequency (Hz)
$n = 6$, $m = 1$ (driven)	134·7	130·9
$n = 6$, $m = 1$ (companion)	134·7	126·2
$n = 5$, $m = 1$	143·2	143·6
$n = 7$, $m = 1$	152·9	148·3

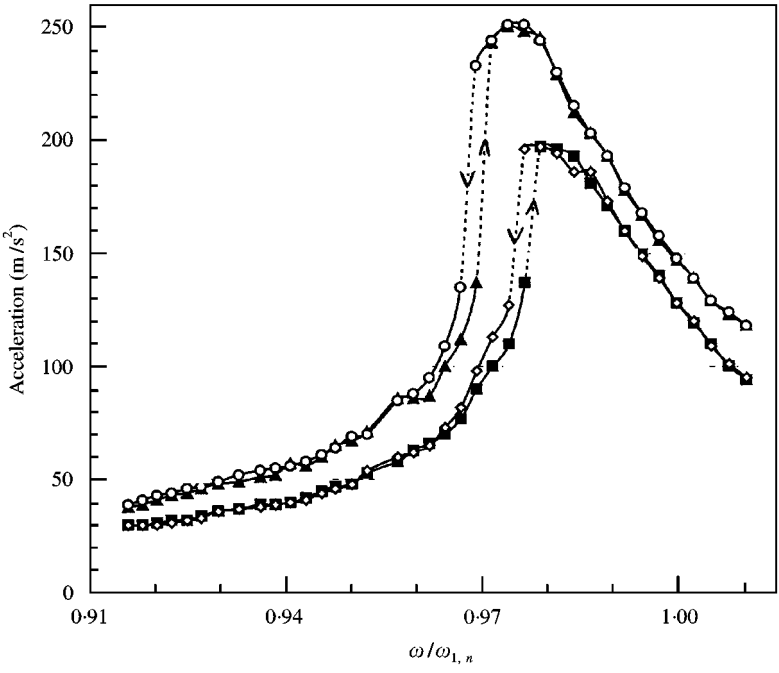

Figure 8. Experimentally measured frequency–response curves for the water-filled test shell. —■—, force level 1·2 N, increasing frequency; —◇—, force level 1·2 N, decreasing frequency; —▲—, force level 1·6 N, increasing frequency; —○—, force level 1·6 N, decreasing frequency.

also theoretically investigated by using the method reported in reference [10]; the frequency of the fundamental mode is lowered by about 4 Hz and the mode shapes are slightly distorted. Acceleration is expected to have different peak values on the anti-nodes as a consequence of distortion of mode shapes. Moreover, this asymmetry of the structure causes a difference between the natural frequencies of the driven and companion modes, as experimentally verified.

Figure 8 shows the accelerations measured by the first accelerometer *versus* the frequency ratio, i.e. excitation frequency/linear frequency of the fundamental mode, for two different force levels: 1·2 and 1·6 N. The measured acceleration was obtained as a peak value of the sinusoidal acceleration. Experiments were performed for both increasing and decreasing excitation frequency, and both curves are given in Figure 8; the hysteresis between the two is clearly visible. The jumps are indicated in the figure with dashed lines. A significant softening behaviour was found. When the vibration amplitude is equal to the shell thickness, the peak of the response appears for a frequency lower by about 2% than that at very low vibration amplitudes.

The accelerations have been converted to displacements, dividing by the squared excitation circular frequency, and have been plotted in Figure 9 together with the theoretical responses without companion mode participation (practically coincident with $A_{1,n}(t)$ in this case), since the companion mode was not observed in the experiments. Theoretical values have been multiplied by 0·94 in order to compare them to the experimental data. The theoretical curves have been computed by using the 6 d.o.f. model, including modes with $2n$ circumferential waves. The damping used to produce the theoretical curves is $\zeta_{1,n} = 0{\cdot}011$, i.e. a damping ratio of 1·1%, which is in good agreement with the experimental values obtained by Amabili [11] for vibrations of a water-filled

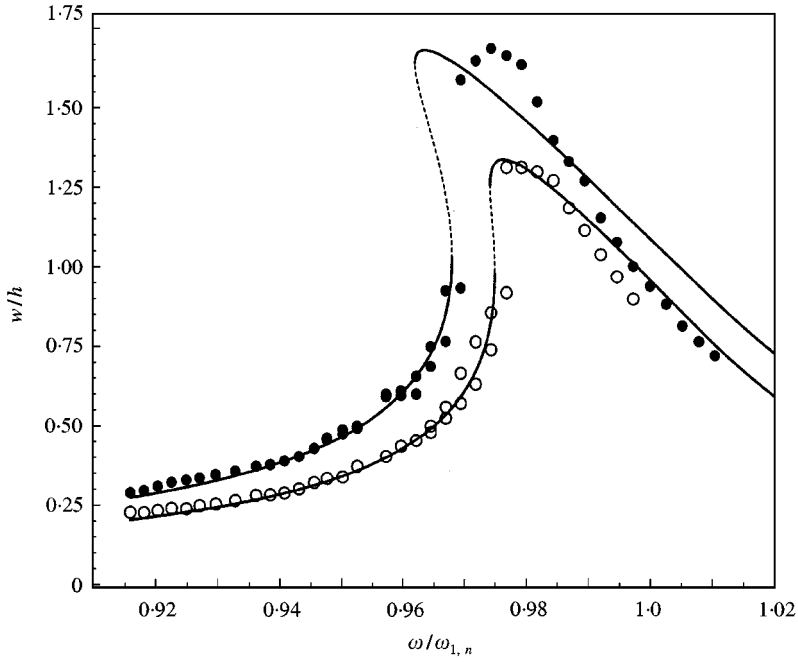

Figure 9. Frequency–response relationship at $x = 0{\cdot}39L$ for the water-filled test shell. ○, experimental data, force level 1·2 N; ●, experimental data, force level 1·6 N; ——, stable theoretical solutions; — — —, unstable theoretical solutions.

circular cylindrical shell made of steel with thin end-plates. The relation $F = f_{1,n}(\pi LR/2)$ [2] can be used to transform the modal excitation, used in the theoretical computations, to a point excitation F (N), to compare to experiments. It must be observed that the experimental forces are smaller than the theoretical ones, because there are additional loads (sensors) on the shell at the force input.

The agreement between the theoretical curves and the experimental results is very good; in particular, it is excellent for the lowest curve. The experimental points in the right-hand part of Figure 9, for both forcing amplitudes, lie to the left of the theoretical curves. This is explained by the presence of another mode, $n = 5$ and $m = 1$, which is very close in frequency to the fundamental mode investigated in the shell tested, as shown in Table 1. Between the two modes an antiresonance has been experimentally detected; this is close enough to the peak of the response of the fundamental mode to modify the experimental response (with at least a linear effect) in the right-hand part of Figure 9. In fact, it is important to clarify, that the theoretical response does not take into account the interaction between the fundamental mode, $n = 6$ and $m = 1$, and the additional mode, $n = 5$ and $m = 1$. Overall, Figure 9 bespeaks of the good accuracy of the model developed in the present series of papers.

Companion mode participation has not been found in the experiments. It has been found experimentally that what should have been the companion mode has in fact a natural frequency about 3% lower than the driven mode (see Table 1), as a consequence of the test-shell being imperfectly axisymmetric due to manufacturing imperfections, the presence of the seam and the sensors attached to the shell. This difference between the natural frequency of the driven and companion mode is the reason for the absence of the companion mode in the experimental response.

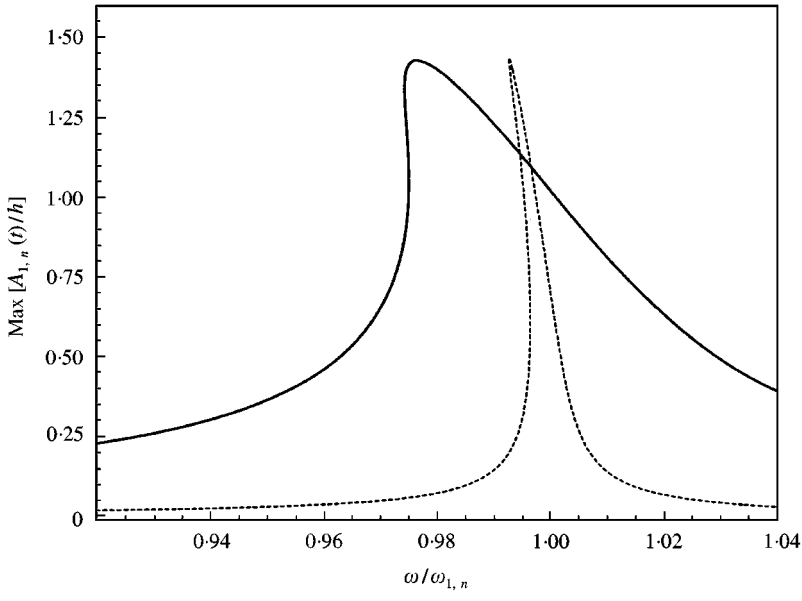

Figure 10. Theoretical frequency–response curve for the test-shell: ——, water-filled shell, excitation $f_{1,n} = 0{\cdot}0354h\omega_{1,n}^2 m_1\,[2/(\pi L)]$, damping $\zeta = 0{\cdot}011$; — — —, empty shell, excitation $f_{1,n} = 0.003h\omega_{1,n}^2 m_1\,[2/(\pi L)]$, damping $\zeta = 0.001$.

Figure 10 presents the theoretical curve shown in Figure 9 for the lowest force level, together with the theoretical response for the same shell, without water, and with a reduced modal damping coefficient $\zeta_{1,n} = 0{\cdot}001$, compatible with structural damping of the test-shell. This figure shows that water contained in the shell generates a much stronger softening behaviour of the system.

6. CONCLUSIONS

Results show that additional asymmetric modes in the mode expansion used in the analysis of forced vibrations of the shell have but a small effect on the trend of non-linearity when compared to the first and third axisymmetric modes. The effect of additional longitudinal modes is absolutely insignificant, in both the driven and companion mode responses. The effect of modes with $2n$ circumferential waves is limited on the trend of non-linearity but is qualitatively significant in the response with companion mode participation, at least for shells with very small damping. In particular, the travelling wave response appears at much lower vibration amplitudes and there is a central area in the frequency–response plane without stable periodic responses, corresponding to a beating phenomenon.

The present results allow us to state that the mode expansions used in references [1, 2] are capable of capturing the shell dynamics with the same accuracy as higher dimensional models, with the exception of an extremely small range of excitation frequency, where the inclusion of modes with $2n$ circumferential waves is essential, at least for shells with very small damping.

A liquid (water) contained in the shell generates a much stronger softening behaviour of the system.

Experiments on a water-filled steel specimen show very good agreement with the theoretical results for the fundamental mode ($n = 6$, $m = 1$) investigated. Vibration amplitudes larger than the shell thickness have been measured and satisfactorily compared, showing a good accuracy of the model developed in the present series of papers. Experimental results show a softening-type non-linearity of about 2% for a vibration amplitude equal to the shell thickness.

ACKNOWLEDGMENTS

This work was partially supported by a grant of the Italian Space Agency (ASI). The last author expresses his gratitude to NSERC of Canada and FCAR of Québec for their support. The first author expresses his gratitude to CNR of Italy for the program of short-term mobility.

REFERENCES

1. M. Amabili, F. Pellicano and M. P. Païdoussis 1999 *Journal of Sound and Vibration* **225**, 655–699. Non-linear dynamics and stability of circular cylindrical shells containing flowing fluid. Part I: stability.
2. M. Amabili, F. Pellicano and M. P. Païdoussis 1999 *Journal of Sound and Vibration* **228**, 1103–1124. Non-linear dynamics and stability of circular cylindrical shells containing flowing fluid, Part II: large amplitude vibrations without flow.
3. H.-N. Chu 1961 *Journal of Aerospace Science* **28**, 602–609. Influence of large amplitudes on flexural vibrations of a thin circular cylindrical shell.
4. M. Amabili, F. Pellicano and M. P. Païdoussis 1998 *Journal of Fluids and Structures* **12**, 883–918. Nonlinear vibrations of simply supported, circular cylindrical shells, coupled to quiescent fluid.
5. M. Amabili, F. Pellicano and M. P. Païdoussis 1999 *Journal of Fluids and Structures* **13**, 785–788. Addendum to "Nonlinear vibrations of simply supported, circular cylindrical shells, coupled to quiescent fluid".
6. J. H. Ginsberg 1973 *Journal of Applied Mechanics* **40**, 471–477. Large amplitude forced vibrations of simply supported thin cylindrical shells.
7. J. C. Chen and C. D. Babcock 1975 *AIAA Journal* **13**, 868–876. Nonlinear vibration of cylindrical shells.
8. S. Wolfram 1996 *The Mathematica Book*. Cambridge, U.K.: Cambridge University Press, third edition.
9. E. J. Doedel, A. R. Champneys, T. F. Fairgrieve, Y. A. Kuznetsov, B. Sandstede and X. Wang 1998 *AUTO* 97: *Continuation and Bifurcation Software for Ordinary Differential Equations* (*with HomCont*), Concordia University, Montreal, Canada.
10. M. Amabili 1996 *Shock and Vibration* **3**, 159–167. Free vibration of a fluid-filled circular cylindrical shell with lumped masses attached, using the receptance method.
11. M. Amabili 1996 *Journal of Sound and Vibration* **191**, 757–780. Free vibration of partially filled, horizontal cylindrical shells.

APPENDIX A: TIME FUNCTIONS USED IN EQUATION (8)

The functions $c_i(t)$, $i = 1, \ldots, 25$, used in equation (8) are given by

$$c_1(t) = A_{1,n}(t)\frac{Eh\pi^2}{L^2R}\Big/\left(\frac{\pi^2}{L^2}+\frac{n^2}{R^2}\right)^2, \quad c_2(t) = B_{1,n}(t)\frac{Eh\pi^2}{L^2R}\Big/\left(\frac{\pi^2}{L^2}+\frac{n^2}{R^2}\right)^2, \tag{A1, A2}$$

$$c_3(t) = A_{1,2n}(t)\frac{Eh\pi^2}{L^2R}\Big/\left(\frac{\pi^2}{L^2}+\frac{4n^2}{R^2}\right)^2, \quad c_4(t) = B_{1,2n}(t)\frac{Eh\pi^2}{L^2R}\Big/\left(\frac{\pi^2}{L^2}+\frac{4n^2}{R^2}\right)^2, \tag{A3, A4}$$

$$c_5(t) = A_{1,0}(t)\frac{EhL^2}{\pi^2 R}, \quad c_6(t) = A_{3,0}(t)\frac{EhL^2}{9\pi^2 R}, \tag{A5, A6}$$

$$c_7(t) = \left[\frac{A_{1,n}^2(t) + B_{1,n}^2(t)}{2} + 2(A_{1,2n}^2(t) + B_{1,2n}^2(t))\right]\frac{Ehn^2L^2}{16\pi^2R^2}, \tag{A7}$$

$$c_8(t) = -[2A_{1,n}(t)A_{1,0}(t) + A_{1,n}(t)A_{1,2n}(t) + B_{1,n}(t)B_{1,2n}(t)]\frac{Eh\pi^2R^2}{4n^2L^2}, \tag{A8}$$

$$c_9(t) = \left[A_{1,n}(t)\left(A_{1,0}(t) - 9A_{3,0}(t) + \frac{9}{2}A_{1,2n}(t)\right) + \frac{9}{2}B_{1,n}(t)B_{1,2n}(t)\right] \times \frac{Ehn^2\pi^2}{2L^2R^2}\Big/\left(\frac{4\pi^2}{L^2} + \frac{n^2}{R^2}\right)^2, \tag{A9}$$

$$c_{10}(t) = 9A_{1,n}(t)A_{3,0}(t)\frac{Ehn^2\pi^2}{2L^2R^2}\Big/\left(\frac{16\pi^2}{L^2} + \frac{n^2}{R^2}\right)^2, \tag{A10}$$

$$c_{11}(t) = -[2B_{1,n}(t)A_{1,0}(t) + A_{1,n}(t)B_{1,2n}(t) - B_{1,n}(t)A_{1,2n}(t)]\frac{Eh\pi^2R^2}{4n^2L^2}, \tag{A11}$$

$$c_{12}(t) = \left[B_{1,n}(t)\left(A_{1,0}(t) - 9A_{3,0}(t) - \frac{9}{2}A_{1,2n}(t)\right) + \frac{9}{2}A_{1,n}(t)B_{1,2n}(t)\right] \times \frac{Ehn^2\pi^2}{2L^2R^2}\Big/\left(\frac{4\pi^2}{L^2} + \frac{n^2}{R^2}\right)^2, \tag{A12}$$

$$c_{13}(t) = 9B_{1,n}(t)A_{3,0}(t)\frac{Ehn^2\pi^2}{2L^2R^2}\Big/\left(\frac{16\pi^2}{L^2} + \frac{n^2}{R^2}\right)^2, \tag{A13}$$

$$c_{14}(t) = (-A_{1,n}^2(t) + B_{1,n}^2(t) - 4A_{1,2n}(t)A_{1,0}(t))\frac{Eh\pi^2R^2}{32n^2L^2}, \tag{A14}$$

$$c_{15}(t) = A_{1,2n}(t)(A_{1,0}(t) - 9A_{3,0}(t))\frac{Ehn^2\pi^2}{8L^2R^2}\Big/\left(\frac{\pi^2}{L^2} + \frac{n^2}{R^2}\right)^2, \tag{A15}$$

$$c_{16}(t) = 18A_{1,2n}(t)A_{3,0}(t)\frac{Ehn^2\pi^2}{L^2R^2}\Big/\left(\frac{16\pi^2}{L^2} + \frac{4n^2}{R^2}\right)^2, \tag{A16}$$

$$c_{17}(t) = (-2A_{1,n}(t)B_{1,n}(t) - 4B_{1,2n}(t)A_{1,0}(t))\frac{Eh\pi^2R^2}{32n^2L^2}, \tag{A17}$$

$$c_{18}(t) = B_{1,2n}(t)(A_{1,0}(t) - 9A_{3,0}(t))\frac{Ehn^2\pi^2}{8L^2R^2}\Big/\left(\frac{\pi^2}{L^2} + \frac{n^2}{R^2}\right)^2, \tag{A18}$$

$$c_{19}(t) = 18B_{1,2n}(t)A_{3,0}(t)\frac{Ehn^2\pi^2}{L^2R^2}\Big/\left(\frac{16\pi^2}{L^2} + \frac{4n^2}{R^2}\right)^2, \tag{A19}$$

$$c_{20}(t) = (-A_{1,n}(t)A_{1,2n}(t) + B_{1,n}(t)B_{1,2n}(t))\frac{Eh\pi^2R^2}{36n^2L^2}, \tag{A20}$$

$$c_{21}(t) = (A_{1,n}(t)A_{1,2n}(t) - B_{1,n}(t)B_{1,2n}(t))\frac{Ehn^2\pi^2}{4L^2R^2}\Big/\left(\frac{4\pi^2}{L^2} + \frac{9n^2}{R^2}\right)^2, \tag{A21}$$

$$c_{22}(t) = (-A_{1,n}(t)B_{1,2n}(t) - B_{1,n}(t)A_{1,2n}(t))\frac{Eh\pi^2R^2}{36n^2L^2}, \tag{A22}$$

$$c_{23}(t) = (A_{1,n}(t)B_{1,2n}(t) + B_{1,n}(t)A_{1,2n}(t))\frac{Ehn^2\pi^2}{4L^2R^2}\Big/\left(\frac{4\pi^2}{L^2} + \frac{9n^2}{R^2}\right)^2, \tag{A23}$$

$$c_{24}(t) = (-A_{1,2n}^2(t) + B_{1,2n}^2(t))\frac{Eh\pi^2R^2}{128n^2L^2}, \quad c_{25}(t) = -2A_{1,2n}B_{1,2n}\frac{Eh\pi^2R^2}{128n^2L^2}. \tag{A24, A25}$$

APPENDIX B: TIME FUNCTIONS USED IN EQUATION (13)

The functions $c_i(t)$, $i = 1, \ldots, 23$, used in equation (13) are given by

$$c_1(t) = A_{1,n}(t)\frac{Eh\pi^2}{L^2R}\Big/\left(\frac{\pi^2}{L^2} + \frac{n^2}{R^2}\right)^2, \quad c_2(t) = B_{1,n}(t)\frac{Eh\pi^2}{L^2R}\Big/\left(\frac{\pi^2}{L^2} + \frac{n^2}{R^2}\right)^2, \tag{B1, B2}$$

$$c_3(t) = A_{3,n}(t)\frac{9Eh\pi^2}{L^2R}\Big/\left(\frac{9\pi^2}{L^2} + \frac{n^2}{R^2}\right)^2, \quad c_4(t) = B_{3,n}(t)\frac{9Eh\pi^2}{L^2R}\Big/\left(\frac{9\pi^2}{L^2} + \frac{n^2}{R^2}\right)^2, \tag{B3, B4}$$

$$c_5(t) = A_{1,0}(t)\frac{EhL^2}{\pi^2R}, \quad c_6(t) = A_{3,0}(t)\frac{EhL^2}{9\pi^2R}, \tag{B5, B6}$$

$$c_7(t) = \left(\frac{A_{1,n}^2(t) + B_{1,n}^2(t)}{2} - A_{1,n}(t)A_{3,n}(t) - B_{1,n}(t)B_{3,n}(t)\right)\frac{Ehn^2L^2}{16\pi^2R^2}, \tag{B7}$$

$$c_8(t) = (A_{1,n}(t)A_{3,n}(t) + B_{1,n}(t)B_{3,n}(t))\frac{Ehn^2L^2}{64\pi^2R^2}, \tag{B8}$$

$$c_9(t) = (A_{3,n}^2(t) + B_{3,n}^2(t))\frac{Ehn^2L^2}{288\pi^2R^2}, \tag{B9}$$

$$c_{10}(t) = -(A_{1,n}(t)A_{1,0}(t) + 9A_{3,n}(t)A_{3,0}(t))\frac{Eh\pi^2R^2}{2L^2n^2}, \tag{B10}$$

$$c_{11}(t) = [A_{1,n}(t)(A_{1,0}(t) - 9A_{3,0}(t)) - A_{3,n}(t)A_{1,0}(t)]\frac{Ehn^2\pi^2}{2L^2R^2}\Big/\left(\frac{4\pi^2}{L^2} + \frac{n^2}{R^2}\right)^2, \tag{B11}$$

$$c_{12}(t) = (9A_{1,n}(t)A_{3,0}(t) + A_{3,n}(t)A_{1,0}(t))\frac{Ehn^2\pi^2}{2L^2R^2}\Big/\left(\frac{16\pi^2}{L^2} + \frac{n^2}{R^2}\right)^2, \tag{B12}$$

$$c_{13}(t) = 9A_{3,n}(t)A_{3,0}(t)\frac{Ehn^2\pi^2}{2L^2R^2}\Big/\left(\frac{36\pi^2}{L^2} + \frac{n^2}{R^2}\right)^2, \tag{B13}$$

$$c_{14}(t) = -(B_{1,n}(t)A_{1,0}(t) + 9B_{3,n}(t)A_{3,0}(t))\frac{Eh\pi^2R^2}{2L^2n^2}, \tag{B14}$$

$$c_{15}(t) = [B_{1,n}(t)(A_{1,0}(t) - 9A_{3,0}(t)) - B_{3,n}(t)A_{1,0}(t)]\frac{Ehn^2\pi^2}{2L^2R^2}\Big/\left(\frac{4\pi^2}{L^2} + \frac{n^2}{R^2}\right)^2, \tag{B15}$$

$$c_{16}(t) = (9B_{1,n}(t)A_{3,0}(t) + B_{3,n}(t)A_{1,0}(t))\frac{Ehn^2\pi^2}{2L^2R^2}\Big/\left(\frac{16\pi^2}{L^2} + \frac{n^2}{R^2}\right)^2, \tag{B16}$$

$$c_{17}(t) = 9B_{3,n}(t)A_{3,0}(t)\frac{Ehn^2\pi^2}{2L^2R^2}\Big/\left(\frac{36\pi^2}{L^2} + \frac{n^2}{R^2}\right)^2, \tag{B17}$$

$$c_{18}(t) = (-A_{1,n}^2(t) + B_{1,n}^2(t) - 9A_{3,n}^2(t) + 9B_{3,n}^2(t))\frac{Eh\pi^2R^2}{32L^2n^2}, \tag{B18}$$

$$c_{19}(t) = (-A_{1,n}(t)A_{3,n}(t) + B_{1,n}(t)B_{3,n}(t))\frac{4Eh\pi^2n^2}{L^2R^2}\Big/\left(\frac{4\pi^2}{L^2} + \frac{4n^2}{R^2}\right)^2, \tag{B19}$$

$$c_{20}(t) = (A_{1,n}(t)A_{3,n}(t) - B_{1,n}(t)B_{3,n}(t))\frac{Eh\pi^2n^2}{L^2R^2}\Big/\left(\frac{16\pi^2}{L^2} + \frac{4n^2}{R^2}\right)^2, \tag{B20}$$

$$c_{21}(t) = -(A_{1,n}(t)B_{1,n}(t) + 9A_{3,n}(t)B_{3,n}(t))\frac{Eh\pi^2R^2}{16L^2n^2}, \tag{B21}$$

$$c_{22}(t) = -(A_{1,n}(t)B_{3,n}(t) + B_{1,n}(t)A_{3,n}(t))\frac{4Eh\pi^2n^2}{L^2R^2}\Big/\left(\frac{4\pi^2}{L^2} + \frac{4n^2}{R^2}\right)^2, \tag{B22}$$

$$c_{23}(t) = (A_{1,n}(t)B_{3,n}(t) + B_{1,n}(t)A_{3,n}(t))\frac{Eh\pi^2n^2}{L^2R^2}\Big/\left(\frac{16\pi^2}{\mathrm{L}^2} + \frac{4n^2}{R^2}\right)^2. \tag{B23}$$